PHYSICAL REVIEW A VOLUME 8, NUMBER 3 SEPTEMBER 1973

Spectroscopy and Collision Theory. II. The Ar Absorption Spectrum[*]

Chia-Ming Lee and K. T. Lu[†]

Department of Physics, The University of Chicago, Chicago, Illinois 60637

(Received 12 March 1973)

A collision-type formalism for spectral theory, described by Lu and applied originally to Xe, is improved and is applied to analyze the strongly perturbed absorption spectrum of Ar. The analysis expresses experimental data in terms of three sets of empirical parameters: five eigenquantum defects μ_α, one 5×5 orthogonal transformation matrix $\mathfrak{U}_{i\alpha}$, and five dipole matrix elements D_α. The energy dependence of the parameters is studied and is found to be approximately linear for the μ_α and insignificant for $\mathfrak{U}_{i\alpha}$ and D_α. With these parameters thus determined by fitting to the experimental data, the mixing coefficients of the Rydberg levels have been determined and their oscillator strength have been predicted and compared with available experimental data.

I. INTRODUCTION

A collision-theory analysis of highly perturbed spectra has been developed by Fano,[1] in a paper (to be called FH) which relies on Seaton's[2] multichannel quantum-defect method (QDM). FH expresses photoabsorption data obtained below, between, and above different ionization limits in terms of three sets of theoretical parameters. These parameters pertain to collisions of an electron with an ion core (atomic or molecular) and characterize the close-coupling eigenchannels of this system. A related paper by Lu[3] (to be called LX) extended FH to a multichannel case and applied it to analyze Xe spectra which involve five strongly perturbed series.

Although the treatment of LX was successful in describing a vast amount of photoabsorption data in a unified way, it had a number of limitations. First, all parameters were treated as if they were independent of energy, although an energy dependence was apparent in the imperfect fitting of the lower-lying levels. Second, LX did not determine uniquely all elements of the transformation matrix $\mathfrak{U}_{i\alpha}$ which connects the channels i of the dissociated system (electron + ion core) with the eigenchannels α of the same system in a close-coupling situation. Finally, the classification of levels provided by LX remained rather qualitative owing to insufficient knowledge of the matrix $\mathfrak{U}_{i\alpha}$.

The present work started with the modest aim of applying the method of LX to analyze the Ar spectra for which very extensive experimental data are available, primarily due to Yoshino.[4] However, in the course of the work, we succeeded in removing various limitations, thus extending the range of application of the formalism.

The method employed in this paper is basically the same as that of LX; moreover, the Ar spectrum has the same structure as that of Xe. Specifically, photoabsorption by Ar in its ground state leads to the same configurations as one finds in Xe, namely, to np^5d or np^5s, $J=1$, odd-parity states belonging to five series, of which three converge to the first ionization limit $I_{3/2}$ and two converge to the second ionization limit $I_{1/2}$.

In treating the energy dependence of the parameters, we found the procedures involving Seaton's B and $\mathcal{G}$ functions[1,2] to be rather unsuitable for Ar, whereas they had proven valuable for Ne.[5] We treated the energy dependence of the parameters by expanding them directly as linear functions of energy without prior elimination of the Coulomb field effects represented by B and $\mathcal{G}$. This aspect of the problem is discussed in Sec. III.

As in LX,[3] we chose the dissociation channels i to be jj coupled. On the other hand, the α channels are much more nearly LS coupled in Ar than in Xe. This permitted us to fit the $\mathfrak{U}_{i\alpha}$ matrix by minimizing the departure of these channels from LS coupling (Sec. IV).

Complete knowledge of the matrix $\mathfrak{U}_{i\alpha}$ has made it possible to characterize each discrete level of the absorption spectrum quantitatively as a superposition of dissociation channels i with mixing coefficients Z_i and alternatively as a superposition of close-coupling eigenchannels α with mixing coefficients $\mathfrak{A}_\alpha$. These coefficients are given in Table II for 20 excited levels.

As in LX we fitted intensity parameters to reproduce the observed intensity profile of the autoionization spectrum. The parameters were then utilized to predict the line intensities in the discrete spectrum. These predictions will be discussed in Sec. V with oscillator strengths determined by electron collision experiments[6] and with optical relative intensities estimated by Yoshino.[4]

Analysis of the absorption spectra of the Ne, Ar, Kr, Xe group by our method has now reached the following stage: The Ne $2p^5ns$ (and also the $2p^5np$) levels have been studied by Starace.[5] Ar is reported in this paper. For Kr the experimental data are too fragmentary to permit a detailed analysis. For Xe we have tried to improve the fit obtained in LX and to interpret it in greater detail but without sufficient success to warrant a new report.

One obvious application of the present treatment of noble gases would be to analyze the carbon group. In particular, the perturbations noticed by Andrew and Meissner[7] in the series $4s^2\,4p\,(^2P)nd$ of GeI are evidently similar to those occurring in the noble gases and should be amenable to a similar treatment. Other spectra (Al, Ba, and Hg) have been analyzed to some extent in this laboratory.

Sec. II will be a brief summary of the necessary analytic formulas. Numerical fitting will be treated in Sec. IV.

II. SUMMARY OF FORMULAS

This section summarized the formulas of LX and extends them as required for our purposes.

The atoms of interest have two ionization limits $I_{1/2}$ and $I_{3/2}$ corresponding to the doublet core states $p^5\,{}^2P_{1/2}$ and ${}^2P_{3/2}$, respectively. Photoionization of the ground state ($p^6\,{}^1S_0$) yields odd-parity states with $J=1$ consisting of the doublet ion and of a continuum electron in $s_{1/2}$, $d_{3/2}$, or $d_{5/2}$ orbits. These states belong to five *dissociation channels* i which will be labeled in the jj-coupling scheme by

$$\begin{array}{llllll} i= & 1 & 2 & 3 & 4 & 5 \\ \text{label} = & (^2P_{1/2})d_{3/2}, & (^2P_{3/2})d_{5/2}, & (^2P_{3/2})d_{3/2}, & (^2P_{1/2})s_{1/2}, & (^2P_{3/2})s_{1/2} \end{array} \qquad (2.1)$$

(these labels are different from those used in LX). The states of the discrete absorption spectrum are often classified into five perturbed Rydberg series, but each state is actually a superposition of all five dissociation channels. The energy E of each state can be separated into the energy I of the ion and the energy ϵ of the excited or ionized electron. It is important that the energy separation differs for different channels. It is written in a.u. as

$$E = I_i + \epsilon_i = I_i - \frac{1}{2\nu_i^2} = \begin{cases} I_{3/2} - \dfrac{1}{2\nu_{3/2}^{\,2}} & (i=2,3,5) \\ I_{1/2} - \dfrac{1}{2\nu_{1/2}^{\,2}} & (i=1,4), \end{cases} \qquad (2.2)$$

where $I_{3/2} < I_{1/2}$ and ν_i is imaginary or real according to whether $\epsilon_i > 0$ or $\epsilon_i < 0$. There are three spectral regions: *discrete, auto-ionization,* and *open continuum,* corresponding to $E < I_{3/2}$, $I_{3/2} < E < I_{1/2}$, and $I_{1/2} < E$, respectively.

The QDM[2] relies on the existence of a distance r_0 between the excited electron and the residual ion such that the interaction is purely Coulomb for $r \geqslant r_0$. For $r \geqslant r_0$, Eq. (2.12) of LX represents the wave function of the excited or ionized atom as a superposition of the wave functions of the five dissociation channels,

$$\Psi = \sum_i \phi_i \Big[\mathfrak{f}(\nu_i, l_i; r) \sum_\alpha \mathfrak{U}_{i\alpha} \cos\pi\mu_\alpha \mathfrak{A}_\alpha - \mathfrak{g}(\nu_i, l_i; r) \sum_\alpha \mathfrak{U}_{i\alpha} \sin\pi\mu_\alpha \mathfrak{A}_\alpha \Big], \qquad r \geqslant r_0 \qquad (2.3)$$

where ϕ_i denotes the wave functions of the residual ion core, of spins, and of the angular part of the excited electron in the ith channel; $\mathfrak{f}(\nu_i, l_i; r)$ and $\mathfrak{g}(\nu_i, l_i; r)$ are regular and irregular Coulomb wave functions[8] for the ith channel. Symmetrization of the coordinate r of the excited electron with those of other electrons included in ϕ is implied in (2.3), though not indicated explicitly. The parameters of (2.3)—five *eigenquantum defects* μ_α and a 5×5 orthogonal *transformation matrix* $\mathfrak{U}_{i\alpha}$—represent boundary conditions on the wave function at $r = r_0$. The index α pertains to the close-coupling eigenchannels which characterize the effect of short-range interactions between the excited electron and the residual ion. These interactions, involving exchange and other electron correlations, prevail in the region $r < r_0$. These *eigenchannels* α are to be identified by fitting the parameters $\mathfrak{U}_{i\alpha}$ and μ_α to the experimental data. The coefficients $\mathfrak{A}_\alpha$ are to be determined by the boundary conditions at $r = \infty$. These conditions are different in the different ranges of the spectrum.

A. Discrete Spectrum, $E < I_{3/2}$

To each discrete state with an energy E corresponds a pair of values $(\nu_{1/2}, \nu_{3/2})$ determined by Eq. (2.2), from the value of E. The main boundary condition on discrete states, that $\Psi \to 0$ as $r \to \infty$, leads to relation (2.18) of LX,

$$\sum_\alpha F_{i\alpha} \mathfrak{A}_\alpha = 0 \quad \text{for all } i, \qquad (2.4a)$$

where

$$F_{i\alpha} = \mathfrak{U}_{i\alpha} \sin\pi(\nu_i + \mu_\alpha). \qquad (2.4b)$$

Equation (2.4a) has the compatibility condition

$$F(\nu_{1/2}, \nu_{3/2}) = \det|F_{i\alpha}| = 0 \qquad (2.5)$$

and the solution

$$\mathfrak{A}_\alpha = C_{i\alpha}(\nu_{1/2}, \nu_{3/2}) / \Big[\sum_\alpha C_{i\alpha}^2(\nu_{1/2}, \nu_{3/2})\Big]^{1/2}, \tag{2.6}$$

where the index i can be chosen arbitrarily for convenience, and the $C_{i\alpha}(\nu_{1/2}, \nu_{3/2})$ is the cofactor of the element of the ith row and αth column of the determinant $|F_{i\alpha}|$.

The pair of values of $\nu_{1/2}$ and $\nu_{3/2}$ corresponding to each energy level must satisfy (2.2) and (2.5) simultaneously. For the nth particular pair $(\nu_{1/2,n}, \nu_{3/2,n})$, the coefficients $\mathfrak{A}_\alpha^{(n)}$ can be obtained according to Eq. (2.6). Since the wave function in Eq. (2.3) is normalized per unit energy in a.u., the normalization integral needs to be worked out. The result given by (3.13) of LX must be generalized when the energy dependence of the parameters cannot be neglected. The more general result, worked out in Appendix A, is

$$\begin{aligned} N_n^2 = \int |\Psi_n|^2 d\tau = {} & \nu_{3/2,n}{}^3 N_{3/2,n} + \nu_{1/2,n}^3 N_{1/2,n} \\ & + \sum_\alpha \frac{d\mu_\alpha}{dE} (\mathfrak{A}_\alpha^{(n)})^2 \\ & + \sum_i \sum_\alpha \sum_\beta \frac{d\mathfrak{U}_{i\alpha}}{dE} \mathfrak{U}_{i\beta} \\ & \times \sin\pi(\mu_\alpha - \mu_\beta) \mathfrak{A}_\alpha^{(n)} \mathfrak{A}_\beta^{(n)}, \end{aligned} \tag{2.7}$$

where

$$\begin{aligned} N_{1/2,n} &= \sum_{i=1,4} \Big[\sum_\alpha \mathfrak{U}_{i\alpha} \cos\pi(\nu_{i,n} + \mu_\alpha) \mathfrak{A}_\alpha^{(n)}\Big]^2, \\ N_{3/2,n} &= \sum_{i=2,3,5} \Big[\sum_\alpha \mathfrak{U}_{i\alpha} \cos\pi(\nu_{i,n} + \mu_\alpha) \mathfrak{A}_\alpha^{(n)}\Big]^2. \end{aligned} \tag{2.8}$$

Therefore, the normalized wave function for $r > r_0$ can be represented as a superposition of the five dissociation channels in the form

$$\bar{\Psi}_n = \Psi_n / N_n = \sum_i \phi_i P_i^{(n)} Z_i^{(n)}, \tag{2.9}$$

where

$$\begin{aligned} P_i^{(n)} = {} & [\nu_{i,n}^2 \tau(l_i + \nu_{i,n} + 1) \tau(\nu_{i,n} - l_i)]^{-1/2} \\ & \times (2r/\nu_{i,n})^{\nu_{i,n}} e^{-r/\nu_{i,n}} \quad \text{for } r \to \infty, \end{aligned} \tag{2.10}$$

and

$$Z_i^{(n)} = (-1)^{l_i + 1} \sum_\alpha \mathfrak{U}_{i\alpha} \cos\pi(\nu_{i,n} + \mu_\alpha) \mathfrak{A}_\alpha^{(n)} / N_n. \tag{2.11}$$

These coefficients Z_i satisfy the following normalization condition[2]

$$\sum_{ij} Z_i \zeta_{ij} Z_j = 1, \tag{2.12a}$$

where

$$\begin{aligned} \zeta_{ij} = {} & \delta_{ij} + [(-1)^{l_i} (2/\pi\nu_i^3)^{1/2} \cos\pi\nu_i] \frac{d}{dE} \\ & \times \Big(\sum_\alpha \mathfrak{U}_{i\alpha} \tan\pi\mu_\alpha \mathfrak{U}_{j\alpha}\Big) [(-1)^{l_j} (2/\pi\nu_j^3)^{1/2} \cos\pi\nu_j]. \end{aligned} \tag{2.12b}$$

This equation establishes a relationship between the five coefficients $Z_i^{(n)}$, which measure the mixing among the *five dissociation channels* (i channels) for the nth state in the region $r > r_0$, and the five coefficients $\mathfrak{A}_\alpha$, which measure the mixing among the *five close-coupling eigenchannels* (α channels). Through this equation, we can connect the present collisional approach to the traditional spectroscopic interpretation in terms of configuration interaction, as will be discussed in Sec. VI.

The oscillator strength, for the nth state, is written as

$$\begin{aligned} f_n &= \frac{2(E_n - E_0) |\sum_\alpha D_\alpha \mathfrak{A}_\alpha^{(n)}|^2}{N_n^2} \\ &= \frac{2(E_n - E_0) |\sum_\alpha D_\alpha \mathfrak{A}_\alpha^{(n)}|^2}{N_{3/2,n}} \\ & \quad \times \Big[\nu_{3/2,n}^3 + \frac{N_{1/2,n}}{N_{3/2,n}} \nu_{1/2,n}^3 + \sum_\alpha \frac{d\mu_\alpha}{dE} (\mathfrak{A}_\alpha^{(n)})^2 \\ & \quad + \sum_i \sum_\alpha \sum_\beta \frac{d\mathfrak{U}_{i\alpha}}{dE} \mathfrak{U}_{i\beta} \sin\pi(\mu_\alpha - \mu_\beta) \mathfrak{A}_\alpha^{(n)} \mathfrak{A}_\beta^{(n)} \Big]^{-1} \end{aligned} \tag{2.13}$$

according to Eq. (3.12) in LX, with the *five dipole-matrix elements* D_α defined in LX. These five dipole matrix elements D_α are regarded in this paper as the energy-independent parameters to be determined by fitting the Beutler-Fano profiles in the auto-ionization region.

B. Auto-ionization Spectrum, $I_{3/2} < E < I_{1/2}$

Following Sec. III B in LX, there are three open dissociation channels, $i = 2, 3, 5$ in the auto-ionization spectrum. Therefore, there shall be three *collision eigenstates*, $\rho = 1, 2, 3$, each collision eigenstate ρ being a superposition of the standing waves of the *three open dissociation channels* with the same *eigenphase shift* $\pi\tau_\rho$.

For each value of $\nu_{1/2}$ corresponding to an energy E, $I_{3/2} < E < I_{1/2}$; the boundary condition for the wave function in Eq. (2.3) at $r = \infty$ will lead to the following relations [see (3.23) of LX]:

$$\begin{aligned} & \sum_\alpha \mathfrak{U}_{i\alpha} \sin\pi(\nu_{1/2} + \mu_\alpha) \mathfrak{A}_\alpha^{(\rho)} = 0 \\ & \qquad \text{for the closed channels, } i = 1, 4 \\ & \sum_\alpha \mathfrak{U}_{i\alpha} \sin\pi(-\tau_\rho + \mu_\alpha) \mathfrak{A}_\alpha^{(\rho)} = 0 \\ & \qquad \text{for the open channels, } i = 2, 3, 5, \end{aligned} \tag{2.14}$$

for each of the three *collision eigenstates* ρ. The compatibility condition of Eq. (2.14) gives a relationship between τ_ρ and $\nu_{1/2}$, having the same form as Eq. (2.5) with $\nu_{3/2}$ replaced by $-\tau_\rho$, namely,

$$F(-\tau_\rho, \nu_{1/2}) = 0 \quad \text{for } \rho = 1, 2, 3. \tag{2.15}$$

[Note that (2.2) would require $\nu_{3/2}$ itself to be imaginary in the autoionization spectrum.] The solution of (2.14) is then

$$\mathfrak{A}_\alpha^\rho = C_{i\alpha}(-\tau_\rho, \nu_{1/2}) / [\sum_\alpha C_{i\alpha}^2(-\tau_\rho, \nu_{1/2})]^{1/2} \quad \text{for } \rho = 1, 2, 3. \qquad (2.16)$$

For a given value of $\nu_{1/2}$, Eq. (2.15) is satisfied by three pairs $(-\tau_\rho, \nu_{1/2})$. For each pair there is a set of coefficients $\mathfrak{A}_\alpha^\rho$. Therefore, the density of oscillator strength in the auto-ionization spectrum can be represented as the sum of contributions corresponding to photoionization into the three collision eigenstates ρ, according to Eq. (3.25) in LX:

$$\frac{df}{dE} = \sum_{\rho=1}^{3} \frac{df^{(\rho)}}{dE}, \qquad (2.17)$$

where

$$\frac{df^{(\rho)}}{dE} = \frac{2(E - E_0) |\sum_\alpha D_\alpha \mathfrak{A}_\alpha^\rho|^2}{N_\rho} \qquad (2.18)$$

and

$$N_\rho = \sum_{i=2,3,5} |\sum_\alpha \mathfrak{U}_{i\alpha} \cos(-\tau_\rho + \mu_\alpha) \mathfrak{A}_\alpha^\rho|^2.$$

The dipole-matrix elements D_α can be determined by fitting the profiles in the auto-ionization spectrum according to Eqs. (2.17) and (2.18).

C. Open-Continuum Spectrum, $I_{1/2} < E$

In this energy range we use the coefficients $\mathfrak{A}_\alpha$, which satisfy the ingoing wave boundary condition at ∞ [Eq. (3.28) in LX]. The oscillator-strength densities of the two photoelectron groups can thus be expressed as

$$\begin{aligned} df_{3/2}/dE &= 2(E - E_0) \sum_{\alpha,\beta} \sum_{i=2,3,5} \mathfrak{U}_{\alpha i}^\dagger \mathfrak{U}_{i\beta} \times \cos\pi(\mu_\alpha - \mu_\beta) D_\alpha D_\beta, \\ df_{1/2}/dE &= 2(E - E_0) \sum_{\alpha,\beta} \sum_{i=1,4} \mathfrak{U}_{\alpha i}^\dagger \mathfrak{U}_{i\beta} \times \cos\pi(\mu_\alpha - \mu_\beta) D_\alpha D_\beta, \end{aligned} \qquad (2.19)$$

according to Eqs. (3.29) and (3.30) in LX. Therefore, the total oscillator-strength density and the branching ratio of the two photoelectron groups can be written as

$$\frac{df_{\text{tot}}}{dE} = \frac{df_{3/2}}{dE} + \frac{df_{1/2}}{dE} = 2(E - E_0) \sum_\alpha D_\alpha^2, \qquad (2.20)$$

and the ratio is

$$\frac{df_{3/2}/dE}{df_{1/2}/dE} = \frac{\sum_{i=2,3,5} \sum_{\alpha,\beta} \mathfrak{U}_{\alpha i}^\dagger \mathfrak{U}_{i\beta} \cos\pi(\mu_\alpha - \mu_\beta) D_\alpha D_\beta}{\sum_{i=1,4} \sum_{\alpha,\beta} \mathfrak{U}_{\alpha i}^\dagger \mathfrak{U}_{i\beta} \cos\pi(\mu_\alpha - \mu_\beta) D_\alpha D_\beta}. \qquad (2.21)$$

From these formulas the Ar experimental uv photoabsorption data on level positions, line intensities, intensity profiles in the auto-ionization spectrum, the total photoabsorption cross section in the open-continuum spectrum, and the branching ratio of the two photoelectron groups can be expressed in terms of three sets of parameters, $(\mathfrak{U}_{i\alpha}, \mu_\alpha, D_\alpha)$, which are slowly-varying functions of energy within the neighborhood of the ionization limits. The energy dependence of these parameters will be discussed in Sec. III.

III. ENERGY DEPENDENCE OF PARAMETERS

All parameters of QDM[2] should be considered as a slowly-varying function of energy within the neighborhood of ionization limits. In Fano's treatment of the H_2 spectrum the energy range of interest was about 4×10^{-3} a.u., near the ionization limits, hence these parameters were regarded to be energy independent. The possible extension to a broader spectral range has been discussed by Fano in Appendix B of FH.[1] Applying this method, Starace[5] has analyzed successfully the spectrum of Ne over the energy range of 1.8×10^{-1} a.u. near the ionization limits. In Lu's treatment[3] of the Xe spectrum, the energy dependence of these parameters has been disregarded over the energy range of 1.8×10^{-1} a.u. near the ionization limits. Nevertheless, only limited evidence has emerged of gross errors due to disregarding the energy dependence of these parameters for Xe. In the present problem of Ar, the energy range is about 1.6×10^{-1} a.u., near the ionization limits. The evidence for the energy dependence of these parameters is quite apparent as will be discussed in Sec. IV. Therefore, the energy dependence has to be taken into account and is going to be discussed in the following.

In the range $r > r_0$, the long-range Coulomb interaction is taken into account by representing the wave function of the excited electron as a linear superposition of analytically known Coulomb functions. The coefficients of this superposition have been related by Seaton[2] to elements of a short-range electron-ion scattering matrix. For this purpose, Seaton used two alternative pairs of Coulomb functions, each of which can serve as a basis for describing an arbitrary state of the electron in Coulomb field. These two pairs of

Coulomb functions denoted by $(\mathfrak{f},\mathfrak{g})$ and (f,g) are related by a linear transformation[8] and coincide at the ionization limit.

The pair of Coulomb functions $(\mathfrak{f},\mathfrak{g})$ forms a convenient basis for representing the wave function in the asymptotic region $r\rightarrow\infty$ over an energy range extending across the ionization limit. With this choice of Coulomb functions, the wave function in the region $r>r_0$ can be represented by Eq. (2.3) with the transformation matrix $\mathfrak{U}_{i\alpha}$ and the eigenquantum defects μ_α as parameters. Fano[1] and Lu[3] have emphasized that these parameters correspond to the eigenvalues and the eigenvectors of a short-range electron-ion scattering matrix (i.e., $S_{ij}=\sum_\alpha \mathfrak{U}_{i\alpha}e^{2i\pi\mu_\alpha}\mathfrak{U}_{\alpha j}^{\dagger}$), and that they represent boundary conditions on the wave functions at $r=r_0$, which characterize the dynamics of the excited electron in the region $r<r_0$. These parameters are expected to depend on energy, since they involve the energy dependence of the boundary conditions of the wave functions and the values of Coulomb function $(\mathfrak{f},\mathfrak{g})$ at $r=r_0$.

The other pair of Coulomb functions (f,g) considered by Seaton is normalized to be energy independent at $r=0$. In fact, these functions are approximately energy independent over the combined range (see Sec. III of Ref. 8):

$$-\bar{\epsilon}<\epsilon<\bar{\epsilon},\quad r\ll 1/\bar{\epsilon}, \tag{3.1}$$

where $\bar{\epsilon}$ is much smaller than the potential and kinetic energies. As stressed by Seaton, f and g are analytic functions of energy ϵ, while $\mathfrak{f}$ and $\mathfrak{g}$ are continuous but nonanalytic functions of ϵ. The representation (2.3) of the wave function in the region $r>r_0$ can be replaced by a similar linear superposition of the Coulomb functions (f,g) with the parameters ξ_β and $U_{i\beta}$. The connection between $(\mathfrak{f},\mathfrak{g})$ and (f,g) establishes an energy-dependent transformation between the two sets of parameters $(\mu_\alpha,\mathfrak{U}_{i\alpha})$ and $(\xi_\beta,U_{i\beta})$; the transformation identifies the index β.[5] The parameters ξ_β and $U_{i\beta}$ correspond to the eigenvalues and eigenvectors of the symmetric matrix IJ^{-1} of Seaton.[2] For practical calculations Seaton introduces the Y matrix which differs from matrix IJ^{-1} by a known function $\mathcal{G}$, $Y=(\mathcal{G}-IJ^{-1})^{-1}$.[2] In his second paper Seaton[9] introduced the concept of representing Y by asymptotic energy expansion together with simple poles. The parameters of the expression of Y as a function of energy were fitted by Moores[10] to experimental discrete levels of the Ca spectrum. Our approach differs from that of Seaton and co-workers[2,9,10] primarily because we fit in effect the eigenvalues and eigenvectors of a scattering matrix, which are smoother functions of energy than the separate elements of the Y matrix. Returning to our study of energy dependence, it has been surmised in FH and in the early phase of this work that the set of parameters $(\xi_\beta,U_{i\beta})$ would vary with energy more slowly than the set $(\mu_\alpha,\mathfrak{U}_{i\alpha})$, because a degree of energy dependence due to motion in the Coulomb field would have been removed by the transformation from $(\mu_\alpha,\mathfrak{U}_{i\alpha})$ to $(\xi_\beta,U_{i\beta})$. In fact, this might be the reason why Starace has analyzed Ne data only for s and p electrons successfully by fitting the parameters $(\xi_\beta,U_{i\beta})$ rather than $(\mu_\alpha,\mathfrak{U}_{i\alpha})$. Note that the difference between (f,g) and $(\mathfrak{f},\mathfrak{g})$ becomes larger as the angular momentum l increases; for $l=0$, the pair (f,g) almost coincide with the pair $(\mathfrak{f},\mathfrak{g})$.[8]

In order to check the above surmise, detailed numerical experiments have been performed on the spectra of Ar and Xe. Our results indicate that in case of Ar, no advantage is achieved by fitting the parameters $(\xi_\beta,U_{i\beta})$ rather than parameters $(\mu_\alpha,\mathfrak{U}_{i\alpha})$, while in case of Xe, the parameters $(\xi_\beta,U_{i\beta})$ are more strongly energy dependent than the parameters $(\mu_\alpha,\mathfrak{U}_{i\alpha})$. This apparent contradiction can be explained as follows.

The values of the cutoff radius r_0, beyond which the interaction between the excited electron and the residual ion is purely Coulombian, can be taken from the Herman-Skillman potential model[11] for each atom, keeping in mind that they are probably underestimated. These values can be entered into Eq. (3.1) to verify whether the Coulomb functions (f,g) are still approximately energy independent at r_0 throughout the energy range of interest, extending from the lowest discrete level to the second ionization limit. The relevant quantities for Ne, Ar, and Xe are shown in Table I.

From the values of the ratios $(r_0\bar{\epsilon})$, the criterion

TABLE I. The relevant quantities of noble gases.

	Ne	Ar	Xe
r_0 (a.u.) Herman–Skillman	1.7	2.6	3.6
Energy range of interest $(\bar{\epsilon})$ (a.u.)	0.18	0.16	0.18
Combined region $(r\ll 1/\bar{\epsilon})$	$r\ll 5.4$	$r\ll 6.3$	$r\ll 5.4$
$r_0\bar{\epsilon}$	0.31	0.41	0.67

for the parameters $(\xi_\beta, U_{i\beta})$ to exhibit minimum energy dependence (i.e., $r_0\bar{\epsilon} \ll 1$) is not well satisfied in any case—Ne, Ar, or Xe, especially—if r_0 is underestimated. Thus we have no definite reason to choose the set of parameters $(\xi_\beta, U_{i\beta})$ to fit the data. We prefer the set of parameters $(\mu_\alpha, \mathfrak{U}_{i\alpha})$ corresponding to the Coulomb functions $(\mathfrak{f}, \mathfrak{g})$, which form a convenient basis for representing the wave function in the form of Eq. (2.3) in the asymptotic region $r \gg r_0$, and for applying the boundary conditions at $r=\infty$.

These parameters—transformation matrix $\mathfrak{U}_{i\alpha}$ and the eigenquantum defects μ_α—will then be treated as slowly-varying functions of energy within the neighborhood of ionization limits. The 5×5 orthogonal matrix $\mathfrak{U}_{i\alpha}$ is conveniently expressed in terms of ten angles, $\theta_k = 1, \ldots, 10$ as detailed in Appendix B. The energy dependence is then taken into account by expanding the eigenquantum defects μ_α and the angles θ_k into powers of the energy ϵ measured from the lowest ionization limit. In the case of Ar, the energy range of interest, extending from the lowest discrete level up to the second ionization limit, is about 0.16 a.u. We use the linear expansion

$$\begin{aligned} \mu_\alpha &= u_\alpha^0 + \epsilon\mu_\alpha^1, \quad \alpha = 1, \ldots, 5, \\ \theta_k &= \theta_k^0 + \epsilon\theta_k^1, \quad k = 1, \ldots, 10. \end{aligned} \tag{3.2}$$

With regard to the dipole-matrix elements D_α, the fitting was not sufficiently accurate to justify the introduction of a nonzero linear coefficient D_α^1.

IV. NUMERICAL FITTING

Experiments on the UV photoabsorption of Ar have determined the following data: (i) the level positions of five Rydberg series belonging to $(3p^5)nd$ or $(3p^5)ns$, $J=1$, odd-parity states with n up to 58[4]; (ii) the photoabsorption cross section in the autoionization spectrum and in the continuous spectrum beyond the second ionization limit[12]; (iii) the branching ratio of photoelectron groups.[13]

In Sec. II, these quantities have been expressed in terms of three sets of theoretical parameters—eigenquantum defect μ_α, transformation matrix $\mathfrak{U}_{i\alpha}$, and dipole-matrix elements D_α. These parameters will now be determined by fitting the experimental data.

As a preliminary, we recall the surmise[14] that the close-coupling eigenchannels would be LS coupled, since the Coulomb interactions between excited and core electrons are stronger than spin-orbit coupling for $r < r_0$. The experience of LX for Xe confirmed that the α channels are approximately LS coupled, and also showed that the quadrupole coupling between s and d channels is rather weak. Accordingly we classify each α channel by approximate quantum numbers (i.e., by spectroscopy symbols):

$$\begin{array}{llllll} \alpha = & 1 & 2 & 3 & 4 & 5 \\ \mathrm{Sym} = & (p^5d)\,{}^3D & (p^5d)\,{}^1P & (p^5d)\,{}^3P & (p^5s)\,{}^3P & (p^5s)\,{}^1P. \end{array} \tag{4.1}$$

It will be convenient to introduce an intermediate basis of channels $\bar{\alpha}$, for which the quantum numbers l ($\equiv s$ and d), L and S are *exact*, and to represent the connection between actual α channels and the $\bar{\alpha}$ channels by an orthogonal matrix $V_{\bar{\alpha}\alpha}$ which should differ only a little from unity. Thus we factor the matrix $\mathfrak{U}_{i\alpha}$ in the form

$$\mathfrak{U}_{i\alpha} = \sum_{\bar{\alpha}} \mathfrak{U}_{i\bar{\alpha}} V_{\bar{\alpha}\alpha}, \tag{4.2}$$

where $\mathfrak{U}_{i\bar{\alpha}}$ tranforms the jj-coupled channels i into the LS-coupled channels $\bar{\alpha}$. This transformation $\mathfrak{U}_{i\bar{\alpha}}$, which does *not* couple s and d channels, is known analytically[15] and is given by

$$\mathfrak{U}_{i\bar{\alpha}} = [(2j_c+1)(2j_e+1)(2L_{\bar{\alpha}}+1)(2S_{\bar{\alpha}}+1)]^{1/2} \begin{Bmatrix} 1 & \frac{1}{2} & j_c \\ l & \frac{1}{2} & j_e \\ L_{\bar{\alpha}} & S_{\bar{\alpha}} & 1 \end{Bmatrix} = \begin{array}{c|ccccc|} & \alpha=1 & 2 & 3 & 4 & 5 \\ \hline i=1 & \sqrt{\frac{1}{2}} & \sqrt{\frac{1}{3}} & \sqrt{\frac{1}{6}} & 0 & 0 \\ 2 & -\sqrt{\frac{1}{10}} & \sqrt{\frac{3}{5}} & -\sqrt{\frac{3}{10}} & 0 & 0 \\ 3 & -\sqrt{\frac{2}{5}} & \sqrt{\frac{1}{15}} & \sqrt{\frac{8}{15}} & 0 & 0 \\ 4 & 0 & 0 & 0 & \sqrt{\frac{2}{3}} & -\sqrt{\frac{1}{3}} \\ 5 & 0 & 0 & 0 & \sqrt{\frac{1}{3}} & \sqrt{\frac{2}{3}} \end{array}, \tag{4.3}$$

where j_c and j_e pertain to the core and to the photoelectron in the i channels. The $V_{\bar{\alpha}\alpha}$ matrix will be fitted numerically.

The matrix factorization (4.2) has an important further advantage due to representing the dipole-matrix elements D_α in the form,

$$D_\alpha = \sum_{\alpha} V_{\alpha\bar{\alpha}}^{\dagger} D_{\bar{\alpha}}. \tag{4.4}$$

Owing to the selection rule that prohibits intercombination lines from the singlet ground state to triplet excited states, we know in advance that the three $D_{\bar{\alpha}}$ pertaining to triplet states ($\bar{\alpha} = 1, 3, 4$)

must vanish. Accordingly only two of the $D_{\bar{\alpha}}$, pertaining to two ^1P states *remain to be fitted* numerically.

a. Graphical representation.[16] The level position of each discrete line can be represented by a pair of numbers $(\nu_{1/2,n}, \nu_{3/2,n})$ from Eq. (2.2). However, levels with $\nu_{3/2,n} > 30$ have been discarded because the determination of the value of $\nu_{3/2,n}$ (modulo 1) becomes inaccurate near the threshold. As an important part of our procedure, each pair $(\nu_{1/2,n}, \nu_{3/2,n})$ is represented graphically by one point in the plot of $-\nu_{3/2}$ (mod 1) vs $\nu_{1/2}$ (mod 1) shown in Fig. 1. Since each pair $(\nu_{1/2,n}, \nu_{3/2,n})$ must satisfy Eqs. (2.2) and (2.5) simultaneously, each point of the plot must lie at the intersection of lines representing these equations. Equation (2.2) is represented in Fig. 1 by a family of nearly straight lines which cross the figure almost diagonally with varying obliquity; Fig. 1 shows only some fragments of these lines. A main objective of the fitting is to determine parameters $(\mu_\alpha, \mathfrak{U}_{i\alpha})$ such that the curve representing Eq. (2.5), $F(\nu_{1/2}, \nu_{3/2}) = 0$, passes as close as possible to all points of Fig. 1.

A look at the figure shows that the points for low-lying discrete levels do not lie on the same curve $F = 0$ as the others; these departures will have to be corrected by introducing the energy dependence of the parameters. The curve $F = 0$ shown in Fig. 1 pertains to the values of the parameters at the threshold $I_{3/2}$ which we call $(\mu_\alpha^0, \mathfrak{U}_{i\alpha}^0)$.

Important applications of the plot "$-\nu_{3/2}$(mod 1) vs $\nu_{1/2}$(mod 1)" have been stressed in LX.

(i) The intersections of the curve $F = 0$ with the diagonal $\nu_{1/2} - \nu_{3/2} = 0$ have the ordinates $-\nu_{3/2}$ (mod 1) $= \mu_\alpha$; therefore their experimental determination yields the values of μ_α directly.

(ii) The slope $\mathcal{S}$ of the curve $F = 0$ at each of these intersections is

$$\mathcal{S}_\alpha = \sum_{i=1,4} \mathfrak{U}_{i\alpha}^2 \Big/ \sum_{i=2,3,5} \mathfrak{U}_{i\alpha}^2 \,. \qquad (4.5)$$

In addition, should the α and $\bar{\alpha}$ channels coincide exactly, the following would also hold.

(a) The slopes (4.5) would be given by (4.2) as

$$\begin{array}{ll} \alpha: & 1\ 2\ 3\ 4\ 5 \\ \mathcal{S}: & 1\ \tfrac{1}{2}\ \tfrac{1}{5}\ 2\ \tfrac{1}{2}, \end{array} \qquad (4.6)$$

(b) The separation of the matrix (4.2) into two submatrices for s and d states would cause the Eq. (2.5), $F = 0$, to factor into separate equations:

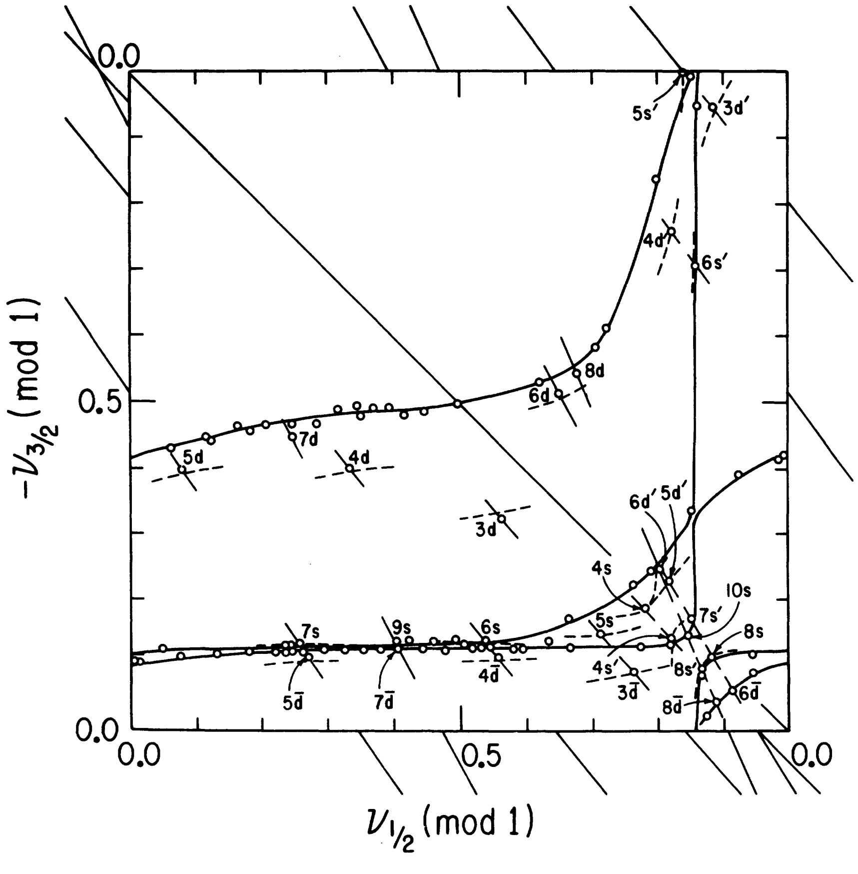

FIG. 1. $-\nu_{3/2}$ (mod 1) vs $\nu_{1/2}$ (mod 1): open circles are observed level positions. Solid curves represent Eq. (2.5), $F = 0$, with parameters fitted near the threshold $I_{3/2}$. The diagonal line represents $\nu_{1/2} - \nu_{3/2} = 0$. The function $-\nu_{3/2}(\nu_{1/2})$ defined by Eq. (2.2) is represented by sections of almost straight oblique lines. Each of the dotted curves represents a section of the curve $F = 0$ fitted to the energy of one of the low-lying levels.

$$F = F_s F_d = 0. \tag{4.7}$$

The curve representing $F = 0$ would then split into two branches that could cross freely. Figure 1 shows that three crossings are narrowly avoided near (0.86, 0.00), (0.86, 0.33), and (0.40, 0.13). The narrowness of the gaps at these quasicrossings indicates that the matrix $V_{\bar{\alpha}\alpha}$ is indeed near unity. This conclusion is confirmed by the fact that the slopes at the intersection with the diagonal are well represented by the values (4.6). Finally, the assumption $V_{\alpha\bar{\alpha}} = \delta_{\alpha\bar{\alpha}}$ leads to a value of 2 for the branching ratio of photoelectron groups (see Sec. VI C of LX); the experimental value of this ratio is indeed 1.98 for Ar, though it was 1.6 for Xe. See however the discussion in the note added in manuscript.

b. Determination of the parameters ($\mu_\alpha^0, U_{i\alpha}^0, D_\alpha$) *at first ionization limit* $I_{3/2}$. We perform here an initial fitting of the parameters using only experimental data within ~0.18 eV of $I_{3/2}$. Values of μ_α^0 can be abtained from the intersection points between the diagonal $\nu_{1/2} - \nu_{3/2} = 0$ and a curve, representing $F(\nu_{1/2}, \nu_{3/2}) = 0$, drawn through the 54 experimental points with $10 < \nu_{3/2} < 30$. The correspondence between each of these intersection points and each of the α labels (4.1) is established using a combination of information from Moore's table,[17] from Hund's rules, and with the help of plots $-\nu_{3/2}$(mod 1) vs $\nu_{1/2}$(mod 1) for other values of J, namely, $J = 0, 2, 3, 4$. These plots are used because the character of the LS-coupled eigenchannels should be the same, irrespective of the J values, as discussed in the Appendix of LX. The values of μ_α^0 have been read off a graph similar to Fig. 1 to an accuracy of ~0.01 and have been assigned to the α channels as follows:

$$\begin{array}{llllll} \alpha = & 1 & 2 & 3 & 4 & 5 \\ \mu_\alpha^0 = & 0.22 & 0.07 & 0.50 & 0.15 & 0.11. \end{array} \tag{4.8}$$

Starting from these values of μ_α^0 and from the trial assumption that $V_{\bar{\alpha}\alpha} = \delta_{\bar{\alpha}\alpha}$, improved values of μ_α^0 and of $V_{\bar{\alpha}\alpha}$ were determined by a least-squares technique with aid of trial values. The quantity to be minimized is

$$\sum_n^{10 < \nu_{3/2,n} < 30} [F(\nu_{3/2,n}, \nu_{1/2,n})]^2, \tag{4.9}$$

with the F function given by (2.5). The numerical work was carried to three significant figures and yielded the more accurate values of μ_α^0, that is

$$\begin{array}{llllll} \alpha = & 1 & 2 & 3 & 4 & 5 \\ \mu_\alpha^0 = & 0.214 & 0.070 & 0.500 & 0.154 & 0.109. \end{array} \tag{4.10}$$

However, it yielded no significant departure of $V_{\bar{\alpha}\alpha}$ from $\delta_{\bar{\alpha}\alpha}$.

We proceed now to the dipole-matrix elements D_α, of which only D_2 and D_5 are nonzero owing to the intercombination selection rule and to $V_{\bar{\alpha}\alpha} \sim \delta_{\bar{\alpha}\alpha}$, as noted above. The parameters D_2 and D_5 were fitted to the intensity profile of the first autoionization line pair above the threshold $I_{3/2}$. This profile, extending over the range $8.64 < \nu_{1/2} < 9.64$, is shown in Fig. 2. The experimental photoabsorption data, from Hudson and Kieffer,[11] are of limited accuracy for the purpose of determining the total oscillator strength owing to intensity saturation in the incompletely resolved very sharp peak. These data were then complemented by the measured total oscillator strength in the smooth continuum just above $I_{1/2}$. [Recall that a series of absorption profiles identical to that of Fig. 2 are observed in each unit range of $\nu_{1/2}$ above 9.64, but that these profiles are increasingly sharp and difficult to resolve as the entire range from $I_{3/2}$ to $I_{1/2}$ extends only over 0.18 eV (1431.4 cm^{-1}).]

The qualitative features of the intensity profile of Fig. 2 are determined primarily by the values of the parameters μ_α^0 and $U_{i\alpha}^0$ and only to a lesser extent by the ratio of the nonzero dipole parameters D_2 and D_5. This ratio has a small influence because an increase of the amplitude D_5 of $p \rightarrow s$ excitation would raise the relative intensity of the sharp peak which is poorly resolved, and hence might escape detection. Actually, the values of μ_α^0 and $U_{i\alpha}^0$ determined by fitting the discrete spectrum account rather well for the qualitative

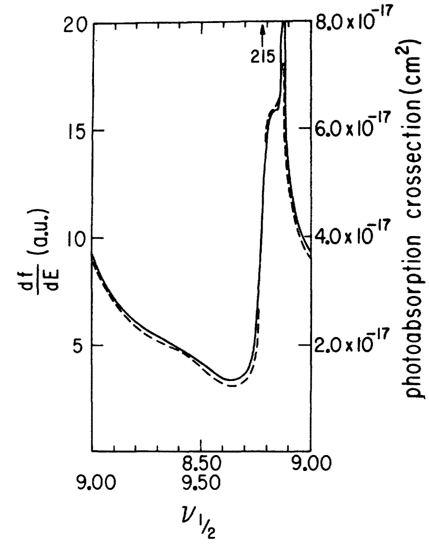

FIG. 2. Argon auto-ionization profile for $8.64 \leq \nu_{1/2} \leq 9.64$ (note abscissa scale mod 1). Dashed lines represent the experimental data from Ref. 12 and solid lines the theoretical fit with D_α listed in (4.12).

features of the profile in Fig. 2. The value of D_2 is then determined primarily by the value of df/dE at any point of the profile, in Fig. 2, far from the sharp peak. The value of D_5 is determined by reconciling the observed height of the sharp peak with the value $df/dE \approx 7.4$ a.u. above the second ionization limit $I_{1/2}$. The D_α parameters thus adopted,

$$\begin{array}{lccccc} \alpha = & 1 & 2 & 3 & 4 & 5 \\ D_\alpha(\text{a.u.}) = & 0 & 2.1 & 0 & 0 & 1.4, \end{array}$$

determine through Eqs. (2.17) and (2.18) the theoretical curve shown in Fig. 2.

As a further step to evaluate the accuracy of fitting, we assumed the value 1.98 observed for the branching ratio (2.21) of photoelectron groups to be significantly different from the value 2. We then again fitted the matrix $V_{\bar{\alpha}\alpha}$, under the assumption of minimum departure of α channels from $\bar{\alpha}$ channels, so that Eq. (2.21) would yield 1.98 without increasing significantly the least-squares-sum value of (4.9). This procedure yielded

$$V_{\bar{\alpha}\alpha} = \begin{vmatrix} 1.000 & 0.001 & 0.000 & 0.000 & 0.001 \\ -0.001 & 1.000 & -0.005 & 0.000 & 0.000 \\ 0.000 & 0.005 & 1.000 & 0.000 & 0.003 \\ 0.000 & 0.000 & 0.000 & 1.000 & 0.000 \\ -0.001 & 0.000 & -0.003 & 0.000 & 1.000 \end{vmatrix},$$

$$\begin{array}{lccccc} \alpha = & 1 & 2 & 3 & 4 & 5 \\ D_\alpha(\text{a.u.}) = & -3.0\times10^{-3} & 2.1 & -2.0\times10^{-2} & 1.0\times10^{-4} & 1.4, \end{array} \qquad (4.12)$$

and left the values (4.10) of μ_α^0 unchanged. In Fig. 1, the curve $F(\nu_{1/2}, \nu_{3/2}) = 0$ calculated by using the adopted parameters $(\mu_\alpha^0, \mathfrak{U}_{i\alpha}^0)$ shows a fair fitting with the experimental points. As shown in Fig. 2, the theoretical autoionization profile, determined by the parameters D_α(4.11), shows no significant difference from the theoretical profile determined by the parameters D_α(4.12). See, however, the discussion in the note added in manuscript.

c. Energy dependence of parameters $(\mu_\alpha, \mathfrak{U}_{i\alpha})$. In Sec. III, the energy dependence of the parameters has been discussed and represented by the linear expansion (3.2). After obtaining the parameters $(\mu_\alpha^0, \mathfrak{U}_{i\alpha}^0)$ at the threshold $I_{3/2}$ from the previous procedures, we now proceed to determine the linear expansion coefficients $(\mu_\alpha^1, \theta_k^1)$.

As noted in Sec. IV a, the five parameters μ_α are determined by the five intersection points between the curve $F = 0$ and the diagonal line $\nu_{1/2} - \nu_{3/2} = 0$ in the plot $-\nu_{3/2}$(mod 1) vs $\nu_{1/2}$(mod 1). The slope of the curve $F = 0$ at each of these five intersections relates to the matrix $\mathfrak{U}_{i\alpha}$ from Eq. (4.5). If now the parameters $(\mu_\alpha, \mathfrak{U}_{i\alpha})$ are energy dependent, the equation $F(\nu_{1/2}, \nu_{3/2}) = 0$ will no longer be represented by a single curve on the $-\nu_{3/2}$(mod 1) vs $\nu_{1/2}$(mod 1) graph of Fig. 1. However, it will be represented by a single curve on a plot of $-\nu_{3/2}$(mod 1) vs $\nu_{1/2}$ itself rather than vs $\nu_{1/2}$(mod 1); such a plot is shown in Fig. 3, where the curve $F(\nu_{1/2}, \nu_{3/2}) = 0$ is simply drawn through the experimental points. As shown in Fig. 3, the point $[\nu_{1/2}, -\nu_{3/2}(\text{mod } 1)]$ representing each discrete level must lie at an intersection of the curve $F(\nu_{1/2}, \nu_{3/2}) = 0$ and of one of the almost straight

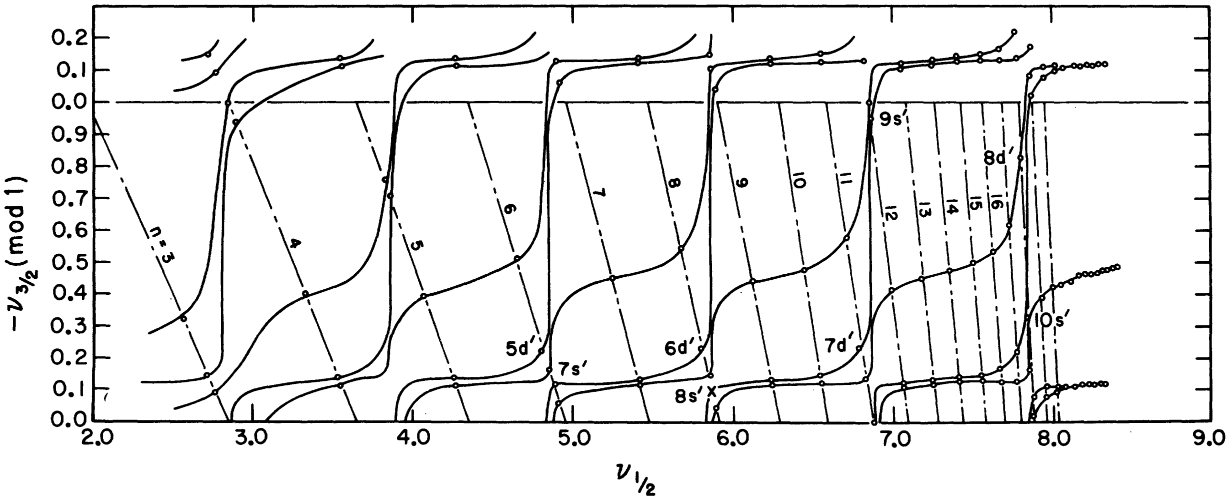

FIG. 3. Quantum defect $-\nu_{3/2}$ (mod 1) vs $\nu_{1/2}$ plot of Ar. Open circles are level positions. The full curves indicate the curve $F = 0$. The relation $-\nu_{3/2}(\nu_{1/2})$ defined by Eq. (2.2) is shown by dot-dashed lines.

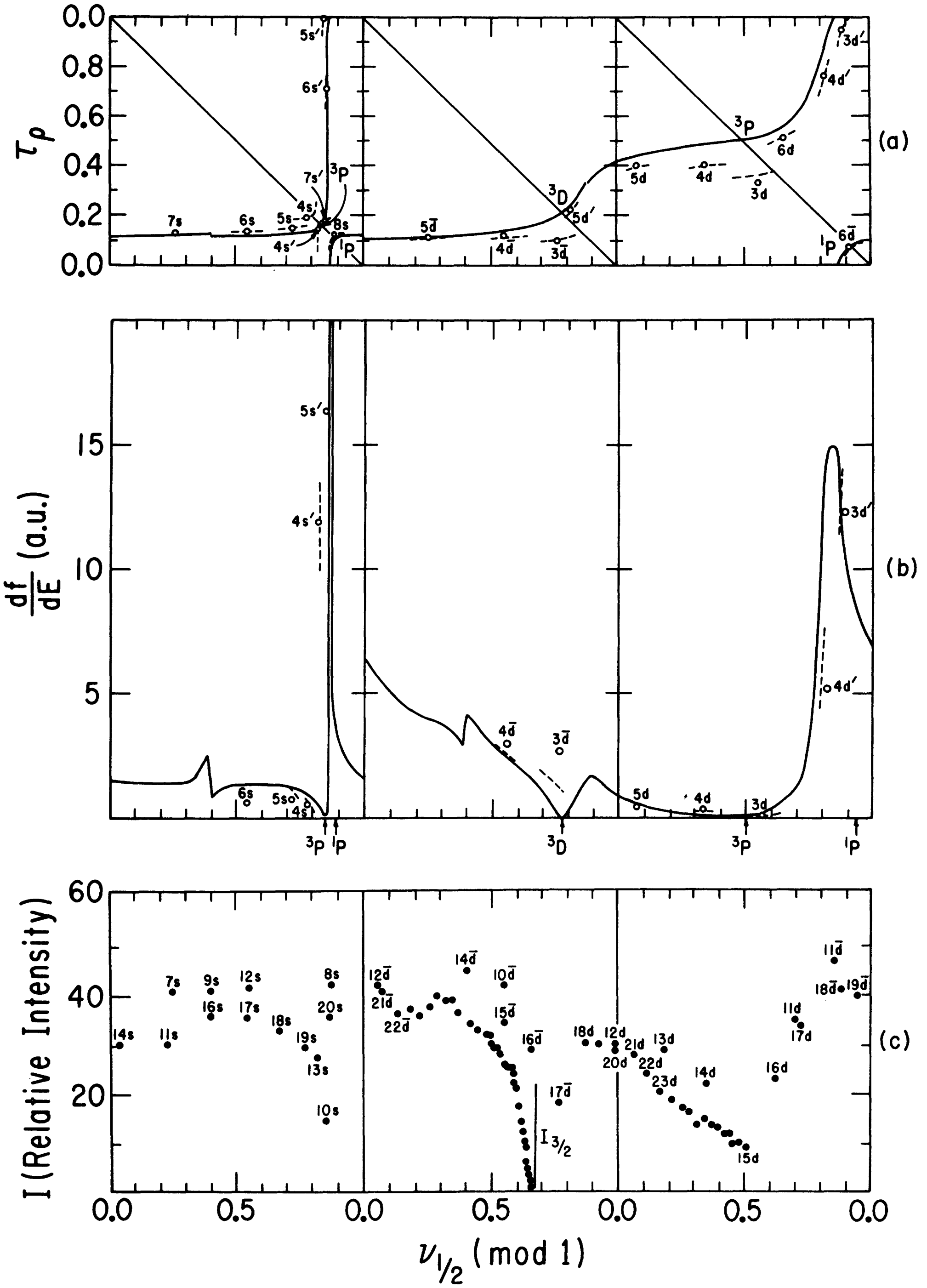

FIG. 4. Eigenphases τ_ρ and oscillator-strength densities $df^{(\rho)}/dE$ for separate eigenchannels $\rho = 1, 2, 3$. (a) Solid lines represent $\tau_\rho(\nu_{1/2})$ for parameters fitted near $I_{3/2}$, dashed lines represent $\tau_\rho(\nu_{1/2})$ for parameters fitted at the $\nu_{1/2}$ value of low-lying lines, and open circles represent experimental data [$\tau_\rho = -\nu_{3/2,n}$ (mod 1)]. (b) Solid lines represent $df^{(\rho)}/dE$ for parameters fitted near $I_{3/2}$, dashed lines represent $df^{(\rho)}/dE$ for parameters fitted at $\nu_{1/2}$ values of low-lying levels, and open circles represent experimental data from Ref. 6 renormalized by Eq. (5.1). (c) Closed circles represent experimental data (relative intensities) from Ref. 4.

lines (2.2) indicated by dashed oblique lines.

To fit the linear expansion coefficients $(\mu_\alpha^1, \theta_k^1)$, we first estimate a set of μ_α^1 from the Fig. 3 and tentatively assign small values to θ_k^1 as trial values. These parameters $(\mu_\alpha^1, \theta_k^1)$ thus can be determined by adjusting these parameters so that the curve $F(\nu_{1/2}, \nu_{3/2}) = 0$, for each of low-lying discrete levels, passes as close as possible to the corresponding experimental point.

The adopted values for the five μ_α^1 are

$$\begin{array}{rccccc} \alpha = & 1 & 2 & 3 & 4 & 5 \\ \mu_\alpha^1(\text{a.u.})^{-1} = & 1.22 & 0.66 & 1.84 & -0.28 & -0.40. \end{array} \tag{4.13}$$

While the ordinates μ_α of the intersection points were thus found to vary appreciably as $\nu_{1/2}$ varies as shown in Fig. 1, the slopes of $F = 0$ at these points remained effectively constant. That is, the values of the parameters θ_k^1 did not depart from zero significantly; in other words, the transformation matrix $\mathfrak{U}_{i\alpha}$ remains approximately the same as the matrix $\mathfrak{U}_{i\alpha}$ at $I_{3/2}$ throughout the range of interest. At this point we may return to the graph of Fig. 1 with $\nu_{1/2}$(mod 1) as the abscissa by folding again the curve $F(\nu_{1/2}, \nu_{3/2}) = 0$ with the values of μ_α given by (4.10) and (4.13); a segment of a curve $F(\nu_{1/2}, \nu_{3/2}) = 0$ for each of low-lying discrete levels, which is calculated by using the adopted parameters, is plotted as a dotted curve in Fig. 1. These curves show a fair fitting with the experimental points except the 3*d* line.

The implications of the parameters $(\mu_\alpha, \mathfrak{U}_{i\alpha}, D_\alpha)$ thus adopted over the whole spectral range of interest will be discussed in Secs. V and VI.

V. ANALYSIS OF OSCILLATOR STRENGTH

Equations (2.13), (2.17), and (2.18) establish the connection between the oscillator strength density df/dE in the auto-ionization spectrum and the oscillator strength f_n of each discrete line. Using the theoretical parameters $(\mu_\alpha, \mathfrak{U}_{i\alpha}, D_\alpha)$ obtained in Sec. IV, and recalling that the D_α have been fitted to the auto-ionization spectrum, we can now predict the values of f_n.

The quantity fitted in the auto-ionization spectrum is the total oscillator-strength density, since the measurements do not separate out the contributions of photoionization to the three collision eigenchannels, $\rho = 1, 2, 3$, Eq. (2.17). However, for the calculation of the f_n we must consider the separate terms of Eq. (2.17). Accordingly, Fig. 4 (b) shows the separate terms $df^{(\rho)}/dE$ for $\rho = 1, 2, 3$, plotted on adjacent graphs; the abscissa of each graph represents one unit range of $\nu_{1/2}$ (mod 1). (The sum of the ordinates of the three graphs coincides with the value of df/dE plotted in Fig. 2.) For purposes of identification, Fig. 4(a) shows the values of τ_ρ for $\rho = 1, 2, 3$, plotted against the same abscissas as $df^{(\rho)}/dE$.

In principle, each curve representing one of the τ_ρ in Fig. 4(a) should coincide with one of the branches of the plot of $-\nu_{3/2}$(mod 1) vs $\nu_{1/2}$(mod 1) in Fig. 1, since the τ_ρ are defined as roots of $F(\nu_{1/2}, -\tau_\rho) = 0$, and the plot of Fig. 1 represents $F(\nu_{1/2}, \nu_{3/2}) = 0$. However we have found it expedient to assign the labels $\rho = 1, 2, 3$ in such a way that the τ_ρ curves skip from one to another branch at the three "near crossing" points with coordinates (0.86, 0.00), (0.86, 0.33), and (0.40, 0.13). This artifice is analogous to the frequent practice of drawing energy-level diagrams of diatomic molecules according to a "diabatic" rather than "adiabatic" approximation. Because of this artifice, the plot of τ_1 represents, in effect, a root of the approximate Eq. (4.7), $F_s(\nu_{1/2}, -\tau_\rho) = 0$, while τ_2 and τ_3 represent roots of $F_d(\nu_{1/2}, -\tau_\rho) = 0$; that is, $\rho = 1$ represents an *s* branch and $\rho = 2, 3$ represent *d* branches. The artifice is justified, in our problem, by the weakness of *sd* coupling discussed in Sec. III. The main result of this artifice of plotting is to smooth out the plots of $df^{(\rho)}/dE$ in Fig. 4(b); a sizeable jag remains for $\rho = 1$ and 2 at the near crossing abscissa $\nu_{1/2} = 0.40$(mod 1), but no visible one appears at the position of the other near crossings.

To calculate the value of f_n for a line of the discrete spectrum with quantum numbers $(\nu_{1/2,n}, \nu_{3/2,n})$ one should take the value of $df^{(\rho)}/dE$ at the abscissa $\nu_{1/2} = \nu_{1/2,n}$ and with such ρ that $\tau_\rho = -\nu_{3/2,n}$ (mod 1) and then divide this value by the coefficient shown in (2.18). The results could then be compared with the experimental values of Ref. 6. Instead we have followed the procedure of LX of renormalizing each experimental value into an effective oscillator-strength density defined by

$$\left(\frac{df}{dE}\right)_n = f_n \left[\nu_{3/2,n}^3 + \nu_{1/2,n}^3 \left(\frac{N_{1/2,n}}{N_{3/2,n}}\right) + \sum_\alpha \frac{d\mu_\alpha}{dE} \left(\mathfrak{A}_\alpha^{(n)}\right)^2 + \sum_i \sum_\alpha \sum_\beta \frac{d\mathfrak{U}_{i\alpha}}{dE} \mathfrak{U}_{i\beta} \sin\pi(\mu_\alpha - \mu_\beta) \mathfrak{A}_\alpha^{(n)} \mathfrak{A}_\beta^{(n)}\right]. \tag{5.1}$$

Each of these renormalized data is plotted in Fig. 4(b) (as marked by circles) at the abscissa for which $\nu_{1/2} = \nu_{1/2,n}$ (mod 1) and $\tau_\rho = -\nu_{3/2,n}$(mod 1).

Also plotted in Fig. 4(b) are theoretical values of the oscillator-strength density adjusted to the low values of $\nu_{1/2} = \nu_{1/2,n}$ pertaining to low-lying discrete levels. The adjustment was made using Eq. (2.18) with the same dipole-matrix elements D_α fitted to the auto-ionization spectrum but taking $\mu_\alpha = \mu_\alpha^0 + \mu_\alpha^1 \epsilon_n$, with $\epsilon_n = -0.5/\nu_{3/2,n}^2$. The calculated values are listed in Table II.

TABLE II. Mixing coefficients $\mathfrak{A}_\alpha$ and Z_i and Ar oscillator strengths.

Moore's designation		$\mathfrak{A}_\alpha$					Z_i							
		1 $(d)\,^3D$	2 $(d)\,^1P$	3 $(d)\,^3P$	4 $(s)\,^3P$	5 $(s)\,^1P$	1 $d(\frac{1}{2},\frac{3}{2})$	2 $d(\frac{3}{2},\frac{5}{2})$	3 $d(\frac{3}{2},\frac{3}{2})$	4 $s(\frac{1}{2},\frac{1}{2})$	5 $s(\frac{3}{2},\frac{1}{2})$	f_n (expt.) [a]	f_n(calc.) [b]	$\left(\frac{df}{dE}\right)_n$(calc.) [c]
$4s[1\frac{1}{2}]^\circ$	$4s$	0.000	0.000	0.003	0.852	0.523	0.001	−0.003	0.003	0.396	0.948	$(7.0 \pm 0.7) \times 10^{-2}$	8.0×10^{-2}	0.6
$4s'[\frac{1}{2}]^\circ$	$4s'$	0.000	0.000	0.001	0.537	−0.844	−0.001	0.001	−0.001	0.946	−0.402	$(2.78 \pm 0.28)\times 10^{-1}$	2.1×10^{-1}	8.8
$3d[\frac{1}{2}]^\circ$	$3d$	−0.126	−0.078	0.989	−0.001	0.000	0.293	−0.526	0.743	0.001	−0.003	$(1.0 \pm 0.1) \times 10^{-3}$	1.6×10^{-3}	0.03
$5s[1\frac{1}{2}]^\circ$	$5s$	−0.030	−0.002	0.001	0.686	0.727	−0.017	0.007	0.020	0.142	0.997	$(2.8 \pm 0.3) \times 10^{-2}$	4.5×10^{-2}	1.1
$3d[1\frac{1}{2}]^\circ$	$3\bar{d}$	−0.866	0.491	−0.089	−0.001	−0.002	−0.357	0.667	0.623	0.000	−0.001	$(9.2 \pm 0.9) \times 10^{-2}$	4.5×10^{-2}	1.3
$5s'[\frac{1}{2}]^\circ$	$5s'$	0.001	0.002	0.001	0.742	−0.670	0.001	−0.002	0.001	0.995	0.146	$(1.24 \pm 0.4) \times 10^{-2}$	3.9×10^{-2}	51.2
$3d'[\frac{1}{2}]^\circ$	$3d'$	0.510	0.840	0.184	−0.006	0.007	0.849	−0.503	0.029	−0.008	−0.002	$(1.10 \pm 0.11)\times 10^{-1}$	1.28×10^{-1}	14.2
$4d[\frac{1}{2}]^\circ$	$4d$	−0.256	−0.154	0.954	−0.002	0.000	0.278	−0.512	0.790	0.001	−0.003	$(4 \pm 1) \times 10^{-3}$	2.6×10^{-3}	0.1
$6s[1\frac{1}{2}]^\circ$	$6s$	−0.001	0.001	0.000	0.612	0.791	0.000	−0.001	0.003	0.069	1.001	$(0.94 \pm 0.7) \times 10^{-2}$	2.3×10^{-2}	1.3
$4d[1\frac{1}{2}]^\circ$	$4\bar{d}$	−0.716	0.690	−0.101	−0.002	−0.003	−0.216	0.774	0.582	0.000	−0.003	$(4.8 \pm 1.4) \times 10^{-2}$	3.9×10^{-2}	2.4
$4d'[\frac{1}{2}]^\circ$	$4d'$	0.639	0.631	0.440	0.006	−0.003	0.875	−0.428	0.200	0.007	−0.001	$(1.5 \pm 0.4) \times 10^{-2}$	3.2×10^{-2}	10.7
$6s'[\frac{1}{2}]^\circ$	$6s'$	−0.005	−0.005	−0.002	0.807	−0.590	−0.007	0.002	0.000	0.998	0.081	$(2.2 \pm 0.4) \times 10^{-2}$	1.3×10^{-2}	161.0
$5d[\frac{1}{2}]^\circ$	$5d$	−0.501	−0.281	0.819	−0.003	0.001	0.359	−0.431	0.818	0.002	−0.003	$(3.2 \pm 0.3) \times 10^{-3}$	$4.3 \quad 10^{-3}$	0.5
$7s[1\frac{1}{2}]^\circ$	$7s$	−0.002	0.001	0.000	0.558	0.830	−0.001	0.000	0.003	0.058	1.000	$(3.7 \pm 1.0) \times 10^{-2}$	1.3×10^{-2}	1.5
$5d[1\frac{1}{2}]^\circ$	$5\bar{d}$	−0.550	0.830	−0.094	−0.002	−0.003	−0.185	0.828	0.523	0.000	−0.003		3.0×10^{-2}	3.6
$6d[\frac{1}{2}]^\circ$	$6d$	0.228	0.157	0.961	0.002	−0.001	0.465	−0.580	0.661	0.003	−0.002		7.5×10^{-4}	0.2
$5d'[\frac{1}{2}]^\circ$	$5d'$	0.990	0.125	−0.059	0.000	0.001	0.657	−0.235	−0.717	0.000	0.000		5.1×10^{-4}	0.18
$7s'[\frac{1}{2}]^\circ$	$7s'$	0.006	−0.001	0.000	0.978	−0.208	0.003	−0.003	−0.006	0.868	0.497		7.4×10^{-4}	0.6
$8s[1\frac{1}{2}]^\circ$	$8s$	0.000	0.000	0.000	−0.105	0.995	0.001	−0.002	0.002	−0.554	0.834		1.3×10^{-2}	3.8
$6d[1\frac{1}{2}]^\circ$	$6\bar{d}$	0.096	0.995	0.025	−0.002	0.003	0.534	0.811	0.232	−0.003	0.002		2.9×10^{-2}	8.5

[a] Experimental oscillator strength from Ref. 6.

[b] Calculated oscillator strength from Eq. (2.13).

[c] Calculated oscillator-strength density from Eq. (5.1).

The experimental points and the calculated value for low-lying lines appear to follow the main features of the main theoretical curve which was based on fitting to the auto-ionization spectrum.

As a further comparison with experimental evidence, we have also entered in Fig. 4(c) Yoshino's[4] experimental "relative line intensities" of highly excited levels of the three Rydberg series converging to $I_{3/2}$. This plot relies on the following considerations.

(i) Each line is unresolved in the spectrogram; accordingly its apparent strength is proportional not to f_n itself, but roughly to the product of f_n and the unresolved width and hence to $f_n \nu^3_{3/2,n}$.

(ii) For large values of $\nu_{3/2,n}$, the last three terms in the brackets of (5.1) are negligible as compared to the first one. Therefore, the relative intensity values given by Yoshino are approximately proportional to $(df/dE)_n$ and are accordingly plotted directly as ordinates in Fig. 4(c).

Interpretation. As shown in Fig. 4(b), the theoretical plot of $df^{(p)}/dE$ reproduces the main features of the variations of $(df/dE)_n$. In particular, it reproduces the points of near-zero intensity which correspond to the three points with "triplet" character among the five intersections between the diagonal $\nu_{1/2} - \nu_{3/2} = 0$ and the curve $F(\nu_{1/2}, \nu_{3/2}) = 0$ as marked in Fig. 4(a). (These zero points of the Ar spectrum were already noted in LX.) Thus the relative intensity for each of the 10s, 15d, 17$\bar{d}$ lines in Fig. 4(c), is very low because these levels are almost pure close-coupling eigenstates with triplet character. The occurrence of these low minima is consistent with the near coincidence of α channels with $\bar{\alpha}$ channels for Ar. We will return to this point with complementary evidence in Sec. VI.

VI. DISCUSSION

Several relationships have been established in this paper between spectral properties of Ar in the discrete and continuum regions. The plot of the equation $F(\nu_{1/2}, \nu_{3/2}) = 0$, in Fig. 1, determines, on the one hand, the position of discrete levels of strongly perturbed series and, on the other hand, the resonant behavior of collision eigenphases $\pi\tau_\rho$ in the auto-ionization region. Figure 4(b) provides the connection between the oscillator strengths in the discrete and the continuum, on the same scale. In all these regards the series of discrete levels and their adjoining continua can be indeed treated as a single unit.

The analytical treatment of this paper involves the parameters μ_α, D_α, and $\mathfrak{U}_{i\alpha}$. Values of these parameters have been obtained by fitting the discrete-level positions, the profile of auto-ionization lines, and the branching ratio in the open continuum, and are given in Eqs. (4.10), (4.12), and (4.13). The energy dependence of these parameters has been represented by expansion as linear functions of energy. Only the eigenquantum defect μ_α appears to be appreciably energy dependent over our spectral range. The over-all fitting is satisfactory except for that of the 3d level in Fig. 1. An expansion including a quadratic energy dependence of μ_α may be required to take care of this low-lying level.

Notice that the eigenquantum defect μ_α decreases with increasing energy in the s series. This downward drift also prevails in other noble gases, e.g., Ne, Kr, and Xe,[5,16,19] and appears to follow the normal trend of scattering phase shifts. That is, the phase shift due to an *attractive* potential (deeper than hydrogenic) is normally a decreasing function of energy except in the vicinity of thresholds or of resonances. By contrast, the presence of a centrifugal potential appears to reverse the situation for the d channels, whose eigenquantum defect μ_α increases with energy.[18,19] This upward drift is most apparent in Ar,[16] less so in Kr,[16] and more or less absent in Xe.[3] This may be correlated with the change in character of the balance between the electrostatic and centrifugal potential.[20] In Ar,[20] this balance creates a well defined potential barrier, which separates two valleys. This barrier confines a 3d electron near the bottom of the outer valley, where the potential is nearly hydrogenic. Increasing excitation permits a d electron to achieve some penetration of the centrifugal barrier toward the inner well where the attraction is much greater than hydrogenic. Thus the eigenquantum defect is larger for high d levels. References 19 and 20, complemented by additional estimates, suggest that the potential barrier is lower in Kr than in Ar and may even disappear for Xe. Accordingly the increase of μ_α with increasing energy, for d electrons, should be reduced along the sequence Ar, Kr, Xe. In fact for Xe all the d levels have approximately the same eigenquantum defect. This might be the reason why a rather satisfactory fitting was obtained for the d levels of Xe even though μ_α was treated as independent of energy. For Ne, the potential for d electrons is almost hydrogenic and therefore the eigenquantum defect is almost zero.

Observable properties have been related in this paper to the five close-coupling eigenchannels α of the complex $e + \mathrm{Ar}^+$. With regard to the eigenchannels α, the electron's orbital momentum is 99.999% $l = 2$, and 0.001% $l = 0$ for three of them, and 99.999% $l = 0$, and 0.001% $l = 2$ for the other two. The s-d interference effects are quite small, being of order ~0.002, as characterized by the smallness of the nonzero elements $\mathfrak{U}_{i\alpha}$ with $i=1,2,3$, $\alpha=5$, which are of the order of 0.2%. Yet the nonzero value of these elements is manifested in the occurrence of avoided crossings between the curves of Fig. 1.

One of the three eigenchannels with predominantly d character, namely the one labeled by $\alpha=2$, is identified as predominantly singlet by the large value of the dipole-matrix parameter D_2 and the large magnitude of the oscillator-strength density at $\nu_{1/2}(\text{mod } 1)=-\mu_2(\text{mod } 1)=0.93$ in Fig. 4. The other singlet is assigned to one of the two eigenchannels with predominantly s character, $\alpha=5$, by the large value of D_5 and large magnitude of oscillator-strength density at $\nu_{1/2}(\text{mod } 1)=-\mu_5(\text{mod } 1)=0.891$. The other three eigenchannels α are identified as triplets as described in Sec. V.

Our data also provide a further characterization of discrete levels through a tabulation of mixing coefficients. Table I gives the components of the eigenvectors $\mathfrak{A}_\alpha$ and Z_i defined in Eq. (2.6) and (2.11). The entries pertain to 20 selected levels listed in order of increasing energy. The coefficients $\mathfrak{A}_\alpha$ and Z_i represent the mixing of α channels and i channels in the given level, respectively. However, they are so normalized according to Eq. [2.12(a)] that $\sum_i Z_i^2$ is not equal to unity for the lower levels. There are five levels, labeled 4s, 5s, 6s, 7s, and 8s, with mixing coefficient $|Z_5|\geq 0.834$; these levels thus belong predominantly to the $i=5$ channel, with a small admixture from the other four i channels, the next more important admixture being from $i=4$. This set of levels represents the $3p^5({}^2P_{3/2})ns\,[1\frac{1}{2}]^\circ$ series according to Moore's assignment. In three of them, $n=5,6,7$, the character is more than 0.99, $i=5$. However, 8s has 0.83 in $i=5$ and a substantial contribution from $i=4$, that is, 8s belongs neither purely to $i=5$ nor to $i=4$. These behaviors reveal themselves in Fig. 4(a), where the ns points with $n=5,6,7$ lie on the flat part of a curve with the same quantum defect and are almost unperturbed. In contrast, 8s lies near the intersection between the diagonal line $\nu_{1/2}-\nu_{3/2}=0$ and the curve $F(\nu_{1/2}-\tau_p)=0$. Table I shows that 8s has the character of $\alpha=5$, i.e., of a singlet state, even though it is *more highly excited* than the ns levels with $n=5,6,7$. Indeed the intensity plot in Fig. 4(b) gives 8s a large oscillator-strength density. For the d levels, we have followed Moore's tables by calling nd, with $n=3,4,5,6$, the levels classified as $3p^5({}^2P_{3/2})nd[\frac{1}{2}]^\circ$, and $n\bar{d}$, with $n=3,4,5,6$, classified as $3p^5({}^2P_{3/2})nd[1\frac{1}{2}]^\circ$. In fact, all of the mixing coefficients Z_i of these levels for $i=1,2,3$ are substantially large. This strong mixing of the i channels constitutes a clear departure from Moore's classification. Indeed most of these levels lie on a rising portion of the curves in Fig. 4(a) rather than on a flat portion. Again, $6\bar{d}$ has the character of a singlet, $\alpha=2$, as one can see both from the table and figure. Thus the combined utilization of Fig. 4 and Table II provides a qualitative and quantitative analysis of strongly perturbed Rydberg spectra of our type.

In the auto-ionization region, the connection between the collisional approach and the traditional interpretation of auto-ionization in terms of configuration interaction,[21] has been developed by Fano[1] for the two-channel problem of H_2. The traditional approach holds only when the resonance profiles are isolated from one another. Otherwise, the collisional approach followed in this paper appears preferable. According to this approach, autoionization of highly excited electrons in the "closed" channels $i=1$ and 4 results from their scattering into the "open" channels $i=2,3,5$ by close range interaction with the Ar^+ core; this scattering is inelastic because it drops the core from its excited doublet level ${}^2P_{1/2}$ to the ground level ${}^2P_{3/2}$. The mixing of *different* eigenchannels α into each state indicates the probability of the scattering from one i channel to another.

The complete fitting of the transformation matrix $\mathfrak{U}_{i\alpha}$ based on minimizing the departure of the α channel from LS coupling, constitutes a novelty of this paper. As a further check of this approach, we examine the relative strength of spin-orbit (so) coupling and electrostatic interaction. In our collision-type method, interaction strengths are represented by dimensionless numerical parameters equal to the shifts of quantum defect $\Delta\mu_{\text{so}}=0.0045$.[22] On the other hand, the eigenquantum-defect differences $\mu_\alpha-\mu_\beta$ of the close-coupling eigenchannels should arise primarily from electrostatic interaction. The smallest difference among the five μ_α in Ar is $\Delta\mu_{2,5}=0.035$, and is thus much larger than $\Delta\mu_{\text{so}}\cong 0.0045$. Also, as we have shown above, the quadrupole coupling between s and d channels is very weak. Therefore the LS characterization for the five α channels is fulfilled. This condition is satisfied even better in Ne; as a matter of fact Starace[5] has assumed complete decoupling of s and d channels. On the other hand, this condition is much less fulfilled for heavier noble gases, e.g., Xe.[3] The procedure for fitting $\mathfrak{U}_{i\alpha}$ developed here can still be applied to situations like that of Xe.

The graphical procedures used in this paper, as well as in LX and FH, apply to spectra with only *two* ionization thresholds in the range of interest. However, the determinant form (2.5) of the $F=0$ equation applies equally to spectra with more than two thresholds, and should be amenable to numerical solution even when the simple graphical approach fails.

Note added in proof. After this work had been completed, we received revised values of the branching ratios of the rare gases (Ne, Ar, Kr, Xe), measured by collecting electrons at the "magic angle" of 54°44′ by Samson.[13] The new branching ratio for Ar is 1.87 ±0.06, instead of the value 1.98 which was utilized by us. This change of the experimental data changes the matrix V [Eq. (4.12)] and the dipole-matrix elements D_α into

$$V_{\bar{\alpha}\alpha}=\left|\begin{array}{ccccc} 1.000 & 0.009 & 0.000 & 0.000 & 0.006 \\ -0.009 & 0.999 & -0.041 & 0.000 & -0.001 \\ 0.000 & 0.041 & 0.999 & 0.000 & 0.027 \\ 0.000 & 0.000 & 0.000 & 1.000 & -0.001 \\ -0.006 & 0.000 & -0.027 & 0.001 & 1.000 \end{array}\right| ,$$

$$\begin{array}{cccccc} \alpha = & 1 & 2 & 3 & 4 & 5 \\ D_\alpha = & -2.8\times10^{-2} & 2.1 & -1.2\times10^{-1} & 1.4\times10^{-3} & 1.4. \end{array}$$

The numerical values on the s-d mixing in the α channels given in Sec. VI are thus changed. However no significant changes result in (i) the $-\nu_{3/2}$ (mod 1) vs $\nu_{1/2}$(mod 1) plot of Fig. 1, up to the second decimal digit included, (ii) the df/dE vs $\nu_{1/2}$(mod 1) plot of Fig. 2, and (iii) the mixing coefficients, $\mathfrak{A}_\alpha$ and Z_i, for s and s' series; changes of the order of ±0.01 do occur in the d, $\bar{d}$, and d' series.

The over-all characterization of the discrete levels discussed in this paper remains thus unaffected. On the other hand, observable quantities which depend sensitively on interferences between different channels are affected by the greater departure of the α channels from the $\bar{\alpha}$ channels. For example, according to Eq. (2.13), the oscillator strengths f_n are proportional to $|\sum_\alpha \mathfrak{A}_\alpha^{(n)} D_\alpha|^2$; the increase of the dipole-matrix element D_3 to reach the order of 10^{-1} a.u. modifies appreciably the small oscillator strengths for the d series given in Table II (see Table III). Other oscillator strengths are not changed significantly.

TABLE III. The corrected oscillator strengths.

	Table II	Corrected
$3d$	1.6×10^{-3}	4.7×10^{-3}
$4d$	2.6×10^{-3}	4.9×10^{-3}
$5d$	4.3×10^{-3}	6.2×10^{-3}
$6d$	7.5×10^{-3}	4.1×10^{-3}

ACKNOWLEDGMENTS

The authors wish to express their deep gratitude to Professor U. Fano for suggesting this problem and for continuous guidance and support. We also wish to thank Dr. A. F. Starace for helpful discussions, and Dr. Dan Dill for the critical reading of the manuscript.

APPENDIX A: NORMALIZATION INTEGRAL

According to the same procedure as in Sec. VI of FH,[1] the normalization integral of the wave function (2.3) can be written as follows:

$$\int^{\infty}\Psi_n^2\,d\tau=\lim_{E\to E_n}\lim_{r\to\infty}\int^{r}\psi\psi_n\,d\tau=\lim_{E\to E_n}\lim_{r\to\infty}(E-E_n)\int^{r}(\psi\psi_n/E-E_n)\,d\tau$$

$$=\frac{1}{\pi}\sum_i\left(\frac{d}{dE}\Big[\sum_\alpha\mathfrak{U}_{i\alpha}\sin\pi(\nu_i+\mu_\alpha)\mathfrak{A}_\alpha\Big]_{E=E_n}\right)\Big[\sum_\alpha\mathfrak{U}_{i\alpha}\cos\pi(\nu_{i,n}+\mu_\alpha)\mathfrak{A}_\alpha^{(n)}\Big]. \tag{A1}$$

For convenience, the normalization integral is decomposed into three contributions with derivatives $d\mathfrak{U}_{i\alpha}/dE$, $d[\sin\pi(\nu_i+\mu_\alpha)]/dE$, and $d\mathfrak{A}_\alpha/dE$, respectively. These three contributions are

$$N_1=\frac{1}{\pi}\sum_i\left(\sum_\alpha\frac{d\mathfrak{U}_{i\alpha}}{dE}\sin\pi(\nu_{i,n}+\mu_\alpha)\mathfrak{A}_\alpha^{(n)}\right)\Big[\sum_\beta\mathfrak{U}_{i\beta}\sin\pi(\nu_{i,n}+\mu_\beta)\mathfrak{A}_\beta^{(n)}\Big]$$

$$=\frac{1}{\pi}\sum_i\left(\sum_\alpha\sum_\beta\frac{d\mathfrak{U}_{i\alpha}}{dE}\mathfrak{U}_{i\beta}\sin\pi(\nu_{i,n}+\mu_\alpha)\cos\pi(\nu_{i,n}+\mu_\beta)\mathfrak{A}_\alpha^{(n)}\mathfrak{A}_\beta^{(n)}\right.$$

$$\left.-\sum_\alpha\sum_\beta\frac{d\mathfrak{U}_{i\alpha}}{dE}\mathfrak{U}_{i\beta}\cos\pi(\nu_{i,n}+\mu_\alpha)\sin(\nu_{i,n}+\mu_\beta)\mathfrak{A}_\alpha^{(n)}\mathfrak{A}_\beta^{(n)}\right)$$

$$=\frac{1}{\pi}\sum_i\sum_\alpha\sum_\beta\frac{d\mathfrak{U}_{i\alpha}}{dE}\mathfrak{U}_{i\beta}\sin\pi(\mu_\alpha-\mu_\beta)\mathfrak{A}_\alpha^{(n)}\mathfrak{A}_\beta^{(n)}, \tag{A2}$$

since

$$\sum_\alpha \mathfrak{U}_{i\alpha} \sin\pi(\nu_{i,n}+\mu_\alpha)\mathfrak{A}_\alpha^{(n)}=0;$$

$$N_2=\frac{1}{\pi}\sum_i\left[\sum_\alpha \mathfrak{U}_{i\alpha}\left(\frac{d}{dE}\sin\pi(\nu_{i,n}+\mu_\alpha)\right)_{E=E_n}\mathfrak{A}_\alpha^{(n)}\right]\left[\sum_\beta \mathfrak{U}_{i\beta}\cos\pi(\nu_{i,n}+\mu_\beta)\mathfrak{A}_\beta^{(n)}\right]$$

$$=\sum_i \nu_{i,n}^3\left[\sum_\alpha \mathfrak{U}_{i\alpha}\cos\pi(\nu_{i,n}+\mu_\alpha)\mathfrak{A}_\alpha^{(n)}\right]^2_{E=E_n}+\sum_i\sum_\alpha\sum_\beta\left(\frac{d\mu_\alpha}{dE}\right)_n \mathfrak{U}_{i\alpha}\mathfrak{U}_{i\beta}\cos\pi(\nu_{i,n}+\mu_\alpha)\cos\pi(\nu_{i,n}+\mu_\beta)\mathfrak{A}_\alpha^{(n)}\mathfrak{A}_\beta^{(n)}$$

$$=\sum_i \nu_i^3\left[\sum_\alpha \mathfrak{U}_{i\alpha}\cos\pi(\nu_{i,n}+\mu_\alpha)\mathfrak{A}_\alpha^{(n)}\right]^2+\sum_i\sum_\alpha\sum_\beta\frac{d\mu_\alpha}{dE}\mathfrak{U}_{i\alpha}\mathfrak{U}_{i\beta}\cos\pi(\mu_\alpha-\mu_\beta)\mathfrak{A}_\alpha^{(n)}\mathfrak{A}_\beta^{(n)}$$

$$=\sum_i \nu_i^3\left[\sum_\alpha \mathfrak{U}_{i\alpha}\cos\pi(\nu_{i,n}+\mu_\alpha)\mathfrak{A}_\alpha^{(n)}\right]^2+\sum_\alpha\frac{d\mu_\alpha}{dE}(\mathfrak{A}_\alpha^{(n)})^2, \tag{A3}$$

since

$$\sum_i \mathfrak{U}_{i\alpha}\mathfrak{U}_{i\beta}=\delta_{\alpha\beta};$$

$$N_3=\frac{1}{\pi}\sum_i\left[\sum_\alpha \mathfrak{U}_{i\alpha}\sin\pi(\nu_{i,n}+\mu_\alpha)\left(\frac{d\mathfrak{A}_\alpha}{dE}\right)_{E=E_n}\right]\left[\sum_\beta \mathfrak{U}_{i\beta}\cos\pi(\nu_{i,n}+\mu_B)\mathfrak{A}_\beta^{(n)}\right]$$

$$=\frac{1}{\pi}\sum_i\sum_\alpha\sum_\beta \mathfrak{U}_{i\alpha}\mathfrak{U}_{i\beta}\sin\pi(\mu_\alpha-\mu_\beta)\left(\frac{d\mathfrak{A}_\alpha}{dE}\right)_{E=E_n}\mathfrak{A}_\beta^{(n)}$$

$$=\frac{1}{\pi}\sum_\alpha\sum_\beta\delta_{\alpha\beta}\sin\pi(\mu_\alpha-\mu_\beta)\left(\frac{d\mathfrak{A}_\alpha}{dE}\right)_{E=E_n}\mathfrak{A}_\beta^{(n)}=0. \tag{A4}$$

Therefore,

$$N_n^2=\int^\infty |\Psi_n|^2 d\tau$$

$$=N_1+N_2+N_3$$

$$=\sum_i \nu_{i,n}^3\left[\sum_\alpha \mathfrak{U}_{i\alpha}\cos\pi(\nu_{i,n}+\mu_\alpha)\mathfrak{A}_\alpha^{(n)}\right]^2$$

$$+\sum_\alpha\frac{d\mu_\alpha}{dE}\mathfrak{A}_\alpha^{(n)2}+\frac{1}{\pi}\sum_i\sum_\alpha\sum_\beta\frac{d\mathfrak{U}_{i\alpha}}{dE}\mathfrak{U}_{i\beta}$$

$$\times\sin\pi(\mu_\alpha-\mu_\beta)\mathfrak{A}_\alpha^{(n)}\mathfrak{A}_\beta^{(n)}. \tag{A5}$$

APPENDIX B: REPRESENTATION OF $n\times n$ ORTHOGONAL MATRIX $\mathfrak{U}$

Geometrically, an $n\times n$ orthogonal matrix describes a rotation in n-dimensional space. Since a rotation in n-dimensional space can be decomposed into a combination of the $\binom{n}{c}$ elementary rotations, $\mathfrak{U}$ can be represented as a vector with $\binom{n}{2}$ components θ_α with the following convention for the subscripts:

$$\begin{array}{lcccccccc}\alpha= & 1 & 2 & \cdots & n-1 & n & \cdots & \frac{1}{2}n(n-1) \\ (i,j)= & (1,2) & (1,3) & \cdots & (1,n) & (2,3) & \cdots & (n-1,n).\end{array}$$

The component θ_α of the vector represents a finite angle of rotation in the (i,j) plane. The explicit expression of $n\times n$ matrix $\mathfrak{U}$ is

$$\mathfrak{U}=n(n-1)/\prod_{\alpha=1}^{2}R^\alpha(\theta_\alpha), \tag{B1}$$

where

$$R^\alpha(\theta_\alpha)=\begin{array}{c|ccccccccccccc|} & 1 & 2 & \cdot & \cdot & i & \cdot & \cdot & \cdot & j & \cdot & \cdot & \cdot & n \\ \hline 1 & 1 & \cdot & \cdot & \cdot & 0 & \cdot & \cdot & \cdot & \cdot & \cdot & \cdot & \cdot & 0 \\ 2 & & 1 & 0 & & \cdot & & & & \cdot & & & & \cdot \\ \cdot & \cdot & & \cdot & & \cdot & & & & \cdot & & & & \cdot \\ \cdot & \cdot & & & 1 & \cdot & & & & \cdot & & & & \cdot \\ i & 0 & \cdot & \cdot & \cdot & \cos\theta_\alpha & 0 & \cdot & \cdot & -\sin\theta_\alpha & \cdot & \cdot & \cdot & 0 \\ \cdot & \cdot & & & & 0 & 1 & & & \cdot & & & & \\ \cdot & \cdot & & & & & & \cdot & & \cdot & & & & \\ \cdot & \cdot & & & & & & & 1 & \cdot & & & & \\ j & 0 & \cdot & \cdot & \cdot & \sin\theta_\alpha & \cdot & \cdot & \cdot & \cos\theta_\alpha & \cdot & \cdot & \cdot & 0 \\ \cdot & \cdot & & & & \cdot & & & & & 1 & & & \cdot \\ \cdot & \cdot & & & & \cdot & & & & & & \cdot & & \cdot \\ \cdot & \cdot & & & & \cdot & & & & & & & \cdot & \cdot \\ n & 0 & \cdot & \cdot & \cdot & 0 & \cdot & \cdot & \cdot & 0 & \cdot & \cdot & \cdot & 1 \end{array}.$$

---

*Work supported by U.S. Atomic Energy Commission under Contract No. C00-1674-77.

†K. T. Lu participated only in the later stages of this work.

[1] U. Fano, Phys. Rev. A **2**, 353 (1970).

[2] M. J. Seaton, Proc. Phys. Soc. Lond. **88**, 801 (1966).

[3] K. T. Lu, Phys. Rev. A **4**, 579 (1971).

[4] K. Yoshino, J. Opt. Soc. Am. **60**, 1220 (1970).

[5] A. F. Starace, J. Phys. B **6**, 76 (1973).

[6] S. Natali, C. E. Kuyatt, and S. R. Mielczarek (unpublished). The line intensities are measured by electron spectroscopy. (We

express our appreciation to Dr. Kuyatt for allowing us use of the data before publication.)

[7] K. L. Andrew and K. W. Meissner, J. Opt. Soc. Am. **49**, 146 (1959).

[8] J. L. Dehmer and U. Fano, Phys. Rev. A **2**, 304 (1970).

[9] M. J. Seaton, Proc. Phys. Soc. Lond. **88**, 815 (1966).

[10] D. L. Moores, Proc. Phys. Soc. Lond. **88**, 843 (1966).

[11] F. Herman and S. Skillman, *Atomic Structure Calculations* (Prentice-Hall, Englewood Cliffs, N.J., 1963).

[12] R. D. Hudson and L. J. Kieffer, At. Data **2**, 205 (1971).

[13] J. A. R. Samson and R. B. Cairns, Phys. Rev. **173**, 80 (1968). We thank Professor Samson for communicating to us his new values of the branching ratio of the rare gases, measured at the "magic angle." The new ratios are Ne = 1.98, Ar = 1.87 ± 0.06, Kr = 1.64, and Xe = 1.44.

[14] U. Fano, Bull. Am. Phys. Soc. **13**, 37 (1968).

[15] U. Fano and G. Racah, *Irreducible Tensorial Sets* (Academic, New York, 1959), p. 68.

[16] K. T. Lu and U. Fano, Phys. Rev. A **2**, 81 (1970).

[17] C. E. Moore, *Atomic Energy Levels*, Natl. Bur. Std. Circ. No. 467 (U.S. GPO, Washington, D.C., 1958), Vol. III.

[18] B. Edlén, *Encyclopedia of Physics* (Springer-Verlag, Berlin, 1964), Vol. 27, p. 80.

[19] E. U. Condon and G. H. Shortley, *Theory of Atomic Spectra* (Cambridge U.P., New York, 1964), p. 143.

[20] A. R. P. Rau and U. Fano, Phys. Rev. **167**, 7 (1968).

[21] U. Fano, Phys. Rev. **124**, 1866 (1961).

[22] U. Fano, Comments At. Mol. Phys. **2** (1), 30 (1970).